

# X-rays from the Mira AB Binary System

Joel H. Kastner<sup>1</sup> and Noam Soker<sup>2</sup>

## ABSTRACT

We present the results of XMM-Newton X-ray observations of the Mira AB binary system, which consists of a pulsating, asymptotic giant branch primary and nearby ( $\sim 0.6''$  separation) secondary of uncertain nature. The EPIC CCD (MOS and pn) X-ray spectra of Mira AB are relatively soft, peaking at  $\sim 1$  keV, with only very weak emission at energies  $> 3$  keV; lines of Ne IX, Ne X, and O VIII are apparent. Spectral modeling indicates a characteristic temperature  $T_X \sim 10^7$  K and intrinsic luminosity  $L_X \sim 5 \times 10^{29}$  erg s<sup>-1</sup>, and suggests enhanced abundances of O and, possibly, Ne and Si in the X-ray-emitting plasma. Overall, the X-ray spectrum and luminosity of the Mira AB system more closely resemble those of late-type, pre-main sequence stars or late-type, magnetically active main sequence stars than those of accreting white dwarfs. We conclude that Mira B is most likely a late-type, magnetically active, main-sequence dwarf, and that X-rays from the Mira AB system arise either from magnetospheric accretion of wind material from Mira A onto Mira B, or from coronal activity associated with Mira B itself, as a consequence of accretion-driven spin-up. One (or both) of these mechanisms also could be responsible for the recently discovered, point-like X-ray sources within planetary nebulae.

*Subject headings:* stars: mass loss — stars: winds, outflows — X-rays: ISM — stars: AGB — stars: magnetic fields

## 1. Introduction

The origin and nature of X-ray emission from highly evolved, post-main sequence stars remains uncertain. In late-type main-sequence stars, X-ray emission is generally assumed

---

<sup>1</sup>Chester F. Carlson Center for Imaging Science, Rochester Institute of Technology, 54 Lomb Memorial Dr., Rochester, NY 14623; jhk@cis.rit.edu

<sup>2</sup>Department of Physics, Technion-Israel Institute of Technology, Haifa 32000, Israel; soker@physics.technion.ac.il

to trace surface magnetic activity ultimately derived from stellar magnetic dynamos. The X-ray detection of several first-ascent red giant stars by ROSAT (e.g., Schröder, Hünsch, & Schmitt 1998; Hünsch et al. 2003) and, more recently, Chandra (Hünsch 2001) therefore suggests that low-mass, post-main sequence stars can be magnetically active (although it is also possible that the X-rays originate from active, main-sequence companion stars). On the other hand, it appears that — despite maser measurements of large local magnetic fields in asymptotic giant branch (AGB) star winds (e.g., Vlemmings, Diamond, & van Langevelde 2002) — single AGB stars are, at best, only weak X-ray sources (Kastner & Soker 2004). This indicates that the surface magnetic fields of AGB stars are locally rather than globally strong (Soker & Kastner 2003, hereafter Paper I, and references therein).

The lack of X-ray emission from AGB stars is intriguing and puzzling, given that several planetary nebulae, as well as certain ionized, bipolar nebulae associated with symbiotic stars, are now known to harbor point-like X-ray emission at their cores (Chu et al. 2001; Guerrero et al. 2001; Kellogg et al. 2001; Kastner et al. 2003). These X-ray sources might be ascribed to PN central stars whose magnetic fields are sufficiently powerful to launch and/or collimate their mass outflows (Blackman et al. 2001a). Alternatively, the X-rays from these systems may originate with binary systems, in which the companion is either accreting material from the mass-losing primary or is itself magnetically active (Guerrero et al. 2001; Soker & Kastner 2002, hereafter SK02). In such systems the presence of an accreting companion, as opposed to magnetic fields on the primary, would explain the collimation of outflows (Soker & Rappaport 2000 and references therein). Blackman et al. (2001b) have proposed that both mechanisms might operate in certain systems that display multipolar symmetry.

The Mira (omicron Ceti) system provides a nearby ( $D \sim 128$  pc) example of a binary system consisting of a mass-losing AGB star and nearby ( $0.6''$  separation) companion (e.g., Karovska et al. 1997). The nature of the companion is uncertain, as its optical through UV spectrum appears to be dominated by emission from an accretion disk that presumably is accumulated from Mira A’s wind (Reimers & Cassatella 1985; Bochanski & Sion 2001; Wood, Karovska & Raymond 2002). The Mira AB system was detected as a weak X-ray source by the Einstein and ROSAT X-ray observatories (Jura & Helfand 1984, hereafter JH84; Karovska et al. 1996) but the origin of this X-ray emission is unknown, given the uncertainty concerning the nature of Mira B. If the X-rays arise from accretion onto Mira B, then the modest X-ray luminosity of the system appears to rule out the possibility that Mira B is a white dwarf (JH84). However, the early Einstein observations of the system lacked the sensitivity and X-ray spectral response to provide a definitive test, in this regard.

In Paper I, we analyzed the archival ROSAT data obtained for Mira AB in the context of the possibility that the X-rays arise in magnetic activity on the AGB star (Mira A). While fits

of coronal plasma models to the ROSAT Position Sensitive Proportional Counter spectrum were consistent with such a hypothesis, these results left open alternative possibilities; for example, the X-ray emission might arise from magnetic activity on Mira B, or from an accretion disk around this companion star. Furthermore, ROSAT lacked hard ( $> 2.5$  keV) X-ray sensitivity.

Here, we report XMM-Newton observations of Mira AB. The sensitivity, energy coverage, and spectral resolution of XMM-Newton far surpass those of Einstein and ROSAT. Hence, these observations allow us to further constrain the various models for the Mira AB system.

## 2. Observations and Data Reduction

XMM-Newton (Jansen et al. 2001) observed the Mira system for 12.22 ks on 2003 July 23. The integration times with the European Photon Imaging Camera (EPIC) MOS and EPIC pn CCD detector systems were 11.97 ks and 10.34 ks, respectively. The spectral resolution of these CCD systems range from  $\sim 50$  eV to  $\sim 150$  eV over the energy range 0.1 – 10 keV. The thick blocking filter was used to suppress optical photons from the Mira system. Standard X-ray event pipeline processing was performed by the XMM-Newton Science Center using version 5.4.1 of the XMM-Newton Science Analysis System (SAS<sup>1</sup>).

The observation resulted in the detection by EPIC of  $\sim 60$  sources in a  $\sim 25' \times 25'$  field centered near the position of Mira A (= HD 14386; SIMBAD position  $\alpha_{J2000} = 02:19:20.7927$ ,  $\delta_{J2000} = -02:58:39.513$ ). These detections include one source (at  $\alpha_{J2000} = 02:19:20.81$ ,  $\delta_{J2000} = -02:58:41.1$ ) that is consistent with the coordinates of the Mira AB system, given the astrometric precision of XMM-Newton (rms pointing uncertainty  $> 3''$  with a median pointing error of  $\sim 1''^2$ ). We are unable to establish whether this emission arises from Mira A or Mira B, as the latter is found only  $0.58''$  from Mira A at position angle  $108^\circ$  (Karovska et al. 1997).

We used SAS and the Interactive Data Language to extract spectra and light curves of this source from the MOS 1, MOS 2, and pn event data within circular regions of radius  $20''$ . Background was determined from an annulus with inner and outer radii of  $20''$  and  $40''$ , respectively (the X-ray count rates in these background regions were comparable to those obtained for regions farther off source). The resulting, background-subtracted count

---

<sup>1</sup><http://xmm.vilspa.esa.es/sas/>

<sup>2</sup><http://xmm.vilspa.esa.es/docs/documents/CAL-TN-0018-2-1.pdf>

rates for the Mira AB system were  $0.027 \pm 0.003 \text{ s}^{-1}$  for MOS 1 and MOS 2 (combined) and  $0.031 \pm 0.003 \text{ s}^{-1}$  for pn.

### 3. Results

#### 3.1. XMM/EPIC X-ray Spectra

In Fig. 1 we display the combined EPIC (MOS 1, MOS2, and pn) counts spectrum of the Mira system. The spectrum peaks at  $\sim 0.9 \text{ keV}$  (top panel), and emission lines of Ne IX, Ne X, and O VIII appear to be present (bottom panel). There is little emission at energies  $> 3 \text{ keV}$ .

We fit the EPIC spectra of the Mira system using XSPEC version 11.2 (Arnaud 1996). SAS was used to construct response matrices and effective area curves for the specific source spectral extraction regions. Motivated by the apparent emission lines of Ne and O in the merged EPIC spectrum, we used a variable-abundance MEKAL model (Kaastra et al. 1996) to fit the spectra (Fig. 2). In our spectral fits, the intervening absorbing column ( $N_H$ ) and X-ray emission temperature ( $T_X$ ) were taken as free parameters as the abundances of individual elements were systematically varied. This procedure was applied during simultaneous fits to the MOS 1, MOS2, and pn spectra, and the results were confirmed via independent fits to each of these three spectra. The best-fit model has an oxygen abundance that is enhanced by a factor  $23 \pm 6$  relative to solar. The fit results further suggest that the Ne and Si abundances may be somewhat enhanced ( $\sim 4$  and  $\sim 2.5$  times solar, respectively, with large uncertainties), while the abundance of Fe is solar (to within the fit uncertainties). These results for the abundances in the X-ray-emitting gas are somewhat tentative, however; the best-fit, variable-abundance model yields  $\chi^2 = 0.81$ , whereas a model with all elemental abundances fixed at solar (for which the best-fit values of  $N_H$  and  $kT_X$  are similar to those of the variable-abundance model) yields  $\chi^2 = 1.27$ .

From the variable-abundance model, we find best-fit values for the intervening absorbing column of  $N_H \approx 4.5 \times 10^{21} \text{ cm}^{-2}$  and X-ray emission temperature of  $T_X \approx 10^7 \text{ K}$ , with formal uncertainties of  $\sim 20\%$ . These results are not very sensitive to the precise values of the abundances in the model. The best-fit model flux is  $6.4 \times 10^{-14} \text{ erg cm}^{-2} \text{ s}^{-1}$  (0.3–3.0 keV), and the intrinsic (unabsorbed) luminosity derived from the model is  $L_X \approx 5 \times 10^{29} \text{ erg s}^{-1}$ . The values for  $T_X$  and source flux derived from the EPIC data are very similar to those derived from model fitting of the ROSAT data for the Mira system (Paper I), while the values of  $N_H$  and  $L_X$  obtained here are somewhat larger than those obtained from the ROSAT data. Fixing  $N_H = 2 \times 10^{21} \text{ cm}^{-2}$  (the value determined from the ROSAT PSPC

data) does not change appreciably the EPIC fit results for  $T_X$ , but would imply that the overabundance of O is much more modest ( $\sim 1.5$  times solar) and, in addition, that Fe may be depleted ( $\sim 0.2$  times solar) in the X-ray-emitting plasma.

We also attempted to fit the EPIC CCD spectra with two-component thermal plasma models wherein  $N_H$  is fixed at  $2 \times 10^{20} \text{ cm}^{-2}$ , the value derived from UV spectral modeling (Wood et al. 2002). We find that the fit in this case essentially reverts to an isothermal model — that is, the “cool” component contributes negligibly to the emission — but with an unrealistically high plasma temperature for the “hot” component. The result is a very poor fit, particularly in the 1 keV region where the Ne lines appear. We conclude that the X-ray-derived value of  $N_H \sim (2 - 5) \times 10^{21} \text{ cm}^{-2}$  is relatively robust.

### 3.2. XMM/EPIC X-ray Light Curve

In Fig. 3, we display the combined EPIC (MOS 1 + MOS 2 + pn) light curve of the Mira system. The EPIC count rate is observed to rise rather abruptly, by a factor  $\sim 2$ , within the first 3 ks of the observation. The X-ray flux then more or less steadily declines, such that by the end of the  $\sim 10$  ks period during which all 3 CCD cameras were active, the count rate had returned approximately to a value at or below that at observation start. The shape of the X-ray light curve is thus suggestive of a magnetic flare or enhanced accretion rate event, although the time interval appears too short to ascertain the quiescent X-ray count rate and, hence, the characteristic flare timescale and amplitude.

## 4. Discussion

Before considering the most likely sources of the X-ray emission from the Mira AB system, we first mention two mechanisms that are unlikely to contribute to this emission. One potential source of X-ray emission is that of collisions between winds from components A and B. It is difficult to estimate the likely X-ray luminosity due to such wind shocks, as the mass loss rate ( $\dot{M}_B$ ) and wind speed ( $v_B$ ) of Mira B appear to be strongly variable (Wood et al. 2002). Recent HST UV observations indicate that  $\dot{M}_B \simeq 5 \times 10^{-13} M_\odot \text{ yr}^{-1}$  and  $v_B = 250 \text{ km s}^{-1}$  whereas earlier IUE observations suggest  $\dot{M}_B \simeq 10^{-11} M_\odot \text{ yr}^{-1}$  and  $v_B = 400 \text{ km s}^{-1}$  (see Fig. 12 in Wood et al. 2002). Nevertheless, adopting these values as representative of high and low states of mass loss from Mira B, we estimate that the shocked wind X-ray luminosity is only  $L_x(\text{wind}) = 5 \times 10^{27} - 2.5 \times 10^{29} \text{ erg s}^{-1}$ , where these estimates are obtained under the assumption that the half of the shocked wind that is expelled toward

Mira A emits X-rays at 100% efficiency. Therefore, as the conversion of wind to radiant energy is probably quite inefficient, the wind shock mechanism is unlikely to account for the measured X-ray luminosity of Mira AB (§3.1).

In addition, the Bondi-Hoyle accretion radius (measured from the center of Mira B) is  $R_{\text{acc}} = 2GM_B/v_r^2 = 18$  AU for reasonable values of the relevant parameters. This is much larger than the stagnation distance of the two winds (measured from the center of Mira B) as given by Wood et al. (2002) for the strong Mira B wind state, i.e.,  $R_s = 3.7$  AU (this value will be lower for the weak Mira B wind state). Thus, the wind from Mira A is more likely to be accreted by Mira B than to collide with the wind blown by Mira B. While this conclusion leads us to propose that the wind from Mira B is a bipolar outflow (perhaps in the form of a collimated fast wind, of the type proposed by Soker & Rappaport 2000), it also casts further doubt on colliding winds as the origin for the X-ray emission. In addition, the apparent X-ray flaring detected here (§3.2) is more consistent with some form of magnetic and/or accretion activity than with wind shocks.

A second possibility is that the X-rays from the system originate with magnetic activity on Mira A (Paper I). In light of our recent XMM-Newton nondetections of X-ray emission from the (apparently single) Mira variables TX Cam and T Cas (Kastner & Soker 2004), such an explanation appears dubious. In addition, the  $\sim 2$  ks timescale of variation in the X-ray emission from the Mira system is much shorter than the characteristic dynamical timescales of AGB stars.

In the remaining discussion, therefore, we only consider processes in which the X-ray emission originates with Mira B or its immediate environment, as is well established in the case of the UV emission from the system (Karovska et al. 1997; Wood et al. 2001). *Chandra* observations of Mira AB at high spatial resolution will provide a crucial test of this hypothesis.

#### 4.1. The X-ray source: implications for the nature of Mira B

The basic physics of accretion of the Mira A wind by Mira B was discussed by JH84. Those authors convincingly argued that the accreting star, Mira B, must be a main sequence star, with a probable mass of  $M_B \simeq 0.5M_\odot$ , and radius  $R_B \simeq 0.6R_\odot$ . The JH84 argument was based in large part on the relatively meager X-ray luminosity of the Mira system; from *Einstein* observations, JH84 derive an X-ray luminosity  $L_x \simeq 3 \times 10^{29}$  erg s $^{-1}$  (0.15–2.5 keV), where we scale their  $L_x$  result for a distance  $D = 128$  pc. This is several orders of magnitude lower than the  $L_x$  expected from the Bondi-Hoyle model of mass accretion onto a white

dwarf (WD) companion, given the mass loss rate and wind speed of Mira (for which JH84 assumed  $\dot{M}_A = 4 \times 10^{-7} M_\odot \text{ yr}^{-1}$  and  $v = 5 \text{ km s}^{-1}$ , respectively, both of which are consistent with more recent observational results; Knapp et al. 1998; Ryde & Schöier 2001).

The results presented in §3.1 confirm the early JH84 results for the  $L_X$  of the Mira system. In particular, although the XMM-Newton results demonstrate that the Mira X-ray source is variable (§3.2), the EPIC data also indicate that there is no appreciable hard ( $E > 2.5 \text{ keV}$ ) X-ray emission from the system. Since the  $L_X$  we and JH84 derive,  $3 - 5 \times 10^{29} \text{ erg s}^{-1}$ , is 1-3 orders of magnitude smaller than the X-ray luminosities typical of accreting WDs in binary (cataclysmic variable) systems (e.g., Pandel et al. 2003; Ramsay et al. 2004) and the X-ray spectrum of Mira AB evidently lacks the high-temperature ( $kT_X > 2 \text{ keV}$ ) component characteristic of such systems, our results strongly support the contention of JH84 that Mira B is exceedingly unlikely to be a WD and is, instead, a low-mass, main sequence star. This conclusion, in turn, has important implications for the nature of the point-like X-ray sources within planetary nebulae. Indeed, such X-ray sources may be very similar in nature to the Mira AB binary and, therefore, also could be powered via one of two alternative, accretion-related mechanisms, as we now describe.

## 4.2. X-rays derived from accretion onto Mira B

Although Mira B is probably not a WD, the X-rays from the Mira system might still be generated through accretion of AGB wind material onto Mira B. The accretion process can produce the X-rays directly, via star-disk interactions, or indirectly, via the spin-up and resulting enhanced magnetic activity of Mira B. Inserting reasonable parameters into equation (4) of SK02, we indeed find that an accretion disk is likely to be formed around a main sequence companion to Mira A, such that either mechanism is viable. We now discuss each process, in turn.

### 4.2.1. *The direct process: magnetospheric accretion*

If Mira B is a late-type star with a magnetically active, convective envelope (see below), then the process of accretion of wind material from Mira A may closely resemble that of magnetospheric accretion onto low-mass, pre-main sequence stars. For such (classical T Tauri) stars, it is generally thought that material flows from accretion disk to star along magnetic field lines (or “funnels”) that are rooted to the stellar surface at high latitudes (e.g., Hayashi et al. 1996; Matt et al. 2002; Kastner et al. 2004; and references therein). In the case

of the Mira system, a magnetospheric origin for X-ray emission via star-disk interactions is favored by the temperature derived from X-ray spectral fitting. This temperature ( $T_X \sim 10^7$  K) is somewhat high to be due to accretion shocks, given the likely free fall velocity of matter onto the surface of a late-type main sequence star (see, e.g., Appendix A of JH84).

The abundance anomalies suggested by the model fits (§3.1) also point to Mira A’s AGB wind material as a likely source of the X-ray-emitting gas. Specifically, the enhanced abundances of O and (possibly) Ne are consistent with the origin of this gas in nuclear processed material dredged up from AGB interior layers (Marigo et al. 1996; Herwig 2004). It is unclear that Mira A is sufficiently massive and/or evolved to have generated excess O and Ne in thermal pulses, however; its 330 d period (Kukarkin et al. 1971) suggests a progenitor mass in the range 1.0–1.2  $M_\odot$  (Jura & Kleinmann 1992), whereas substantial O and Ne production likely requires a progenitor of mass  $> 2 M_\odot$  (Marigo et al.).

Another argument in support of the origin of the X-ray emission in accretion processes is the result  $N_H > 2 \times 10^{21} \text{ cm}^{-2}$ , derived from model fitting of both ROSAT and XMM data (Paper I and §3.1). This X-ray-derived  $N_H$  is a factor  $> 20$  larger than the neutral H absorbing column determined from analysis of the H I Ly  $\alpha$  line (Wood et al. 2002). This discrepancy suggests that the UV and X-ray emission arise in different zones around Mira B and, specifically, that the X-ray-emitting region may be embedded within accretion streams that effectively attenuate the X-rays, as described by JH84.

If the X-rays are indeed generated directly by accretion onto Mira B, then the similarity of the X-ray fluxes as measured in 1993 (by ROSAT) and in 2003 (by XMM) would suggest that the rate of accretion has recovered from the relatively low levels measured (via UV observations) in 1999–2001 (see Wood & Karovska 2004 and references therein).

#### 4.2.2. *The indirect process: spin-up of Mira B*

Alternatively, the X-ray emission from the Mira system may be derived from the spin-up — and resulting increase in magnetic activity — of Mira B, caused by accretion of mass and angular momentum from the AGB wind of Mira A. Such a process has been described by Jeffries, Burleigh, & Robb (1996), Jeffries & Stevens (1996) and SK02. In SK02 (§2.1.1), we conclude that to generate an X-ray luminosity of  $L_x \simeq 5 \times 10^{29} \text{ erg s}^{-1}$  via magnetic activity, a main sequence star of spectral type M4 to F7 (i.e., in the mass range  $0.3M_\odot \lesssim M_B \lesssim 1.3M_\odot$ ) has to be spun up to a period of  $P \lesssim 3$  days, corresponding to an equatorial rotation speed of  $v_{\text{rot}} \gtrsim 15 - 20 \text{ km s}^{-1}$ . Because we expect an accretion disk to be formed around Mira B, we can use equation (6) of SK02 to estimate the rotation velocity of Mira B. That equation



neglects the initial angular momentum of the accreting main sequence star, and assumes that the entire angular momentum of the star comes from mass accreted from an accretion disk, with a Bondi-Hoyle mass accretion rate (including initial angular momentum will increase the rotation rate). Scaling with the parameters mentioned above, and an orbital separation  $a = 100$  AU (somewhat larger than the projected separation of 70 AU; Karovska et al. 1997), we find

$$v_{\text{rot}} \simeq 20 \frac{\Delta M_{\text{AGB}}}{0.3 M_{\odot}} \left( \frac{M_B}{0.5 M_{\odot}} \right)^{3/2} \left( \frac{R_B}{0.6 R_{\odot}} \right)^{-1/2} \left( \frac{a}{100 \text{ AU}} \right)^{-2} \left( \frac{v_r}{7 \text{ km s}^{-1}} \right)^{-4} \text{ km s}^{-1}, \quad (1)$$

where  $\Delta M_{\text{AGB}}$  is the total mass lost by Mira A during its AGB phase (when its wind speed remains low). Hence, Mira B could have accreted sufficient angular momentum to spin fast enough to be magnetically active at levels sufficient to explain the observed  $L_x \sim 5 \times 10^{29} \text{ erg s}^{-1}$ . The lack of significant emission at energies  $E > 3 \text{ keV}$  would make Mira B somewhat unusual among highly active coronal sources, however (e.g., Huenemoerder et al. 2003).

We acknowledge support for this research provided by NASA/GSFC XMM-Newton General Observer grant NAG5–13158 to RIT. N.S. acknowledges support from the Israel Science Foundation. We thank Falk Herwig and Norbert Schulz for useful comments and suggestions.

## REFERENCES

- Arnaud, K. 1996, in “Astronomical Data Analysis Software and Systems V,” eds. G.H. Jacoby & J. Barnes, ASP Conf. Ser. Vol. 101, p. 17
- Blackman, E.G., Frank, A., Markiel, J.A., Thomas, J.H., & Van Horn, H.M. 2001a, *Nature*, 409, 485
- Blackman, E.G., Frank, A., & Welch, C. 2001b, *ApJ*, 546, 288
- Bochanski, J. J., & Sion, E. M. 2001, *BAAS*, 198.1208
- Chu, Y.-H., Guerrero, M.A., Gruendl, R.A., Williams, R.M., & Kaler, J.B. 2001, *ApJ*, 553, L69
- Guerrero, M.A., Chu, Y.-H., Gruendl, R.A., Williams, R.M., & Kaler, J.B. 2001, *ApJ*, 553, L55
- Hayashi, M., Shibata, K., & Matsumoto 1996, *ApJ*, 468, L37
- Huenemoerder, D.P., Canizares, C.R., Drake, J.J., & Sanz-Forcada, J. 2003, *ApJ*, 595, 1131

- Herwig, F. 2004, ApJS, submitted
- Hünsch, M. 2001, in *Astronomical Gesellschaft Abstract Ser.*, Vol. 18, MS 07 10
- Hünsch, M., Konstantinova-Antova, R., de Medeiros, J.-R., Kolev, D., Schmitt, J. H. 2003, in *Stars as Suns: Activity, Evolution and Planets*, IAU Symp. no. 219, held 21-25 July, 2003 in Sydney, Australia
- Jansen, F., et al. 2001, A&A, 365, L1
- Jeffries, R. D., Burleigh, M. R., & Robb, R. M. 1996, A&A, 305, L45
- Jeffries, R. D., & Stevens, I. R. 1996, MNRAS, 279, 180
- Jura, M., & Helfand, D. J. 1984, ApJ, 287, 785 (JH84)
- Jura, M., & Kleinmann, S.G. 1992, ApJS, 79, 105
- Karovska, M., Hack, W., Raymond, J., & Guinan, E. 1997, ApJ, 482, L175
- Karovska, M., Raymond, J., & Guinan, E. 1996, Technical Report, Smithsonian Astrophysical Observatory
- Kaastra, J.S., Mewe, R., Nieuwenhuijzen, H. 1996, in “UV and X-ray Spectroscopy of Astrophysical and Laboratory Plasmas,” eds. K. Yamashita & T. Watanabe (Tokyo : Univ. Acad. Press), p. 411
- Kastner, J. H., Balick, B., Blackman, E. G., Frank, A., Soker, N., Vrtilik, S. D., & Li, J. 2003, ApJ, 591, L37
- Kastner, J. H., & Soker, N. 2004, ApJ, in press (astro-ph/0403063)
- Kastner, J. H., et al. 2004, Nature, submitted
- Kellogg, E., Pedelty, J.A., & Lyon, R.G., ApJ, 563, L151
- Knapp, G. R., Young, K., Lee, E., & Jorissen, A. 1998, ApJS, 117, 209
- Kukarkin, B.V., Kholopov, P.N., Pskovsky, Y.P., Efremov, Y.N., Kukarkina, N.P., Kurochkin, N.E., & Medvedeva, G.I. 1971, *General Catalogue of Variable Stars*, 3rd ed.
- Marigo, P., Bressan, A., & Chiosi, C. 1996, A&A 313, 545
- Matt, S., Goodson, A.P., Winglee, R.M., Bohm, K.-M. 2002, ApJ, 574, 232
- Pandel, D., Cordova, F.A., & Howell, S.B. 2003, MNRAS, 346, 1231
- Ramsay, G., Cropper, M., Mason, K. O., Crdova, F. A., & Priedhorsky, W. 2004, MNRAS, 347, 95
- Reimers, D., & Cassatella, A. 1985, ApJ, 297, 275
- Ryde, N., & Schöier, F. L. 2001, ApJ, 547, 384

- Schröder, K.-P., Hünsch, M., & Schmitt, J. H. M. M. 1998, *A&A*, 335, 591
- Soker, N., & Kastner, J. H. 2002, 570, 245 (SK02)
- Soker, N., & Kastner, J. H. 2003, *ApJ*, 592, 498 (Paper I)
- Soker, N., & Rappaport, S. 2000, *ApJ*, 538, 241
- Vlemmings, W. H. T., Diamond, P. J., & van Langevelde H. J. 2002, *A&A*, 394, 589
- Wood, B. E., & Karovska 2004, *ApJ*, 601, 502
- Wood, B. E., Karovska, M., & Hack, W. 2001, *ApJ*, 556, L51
- Wood, B. E., Karovska, M., & Raymond, J. C. 2002, *ApJ*, 575, 1057

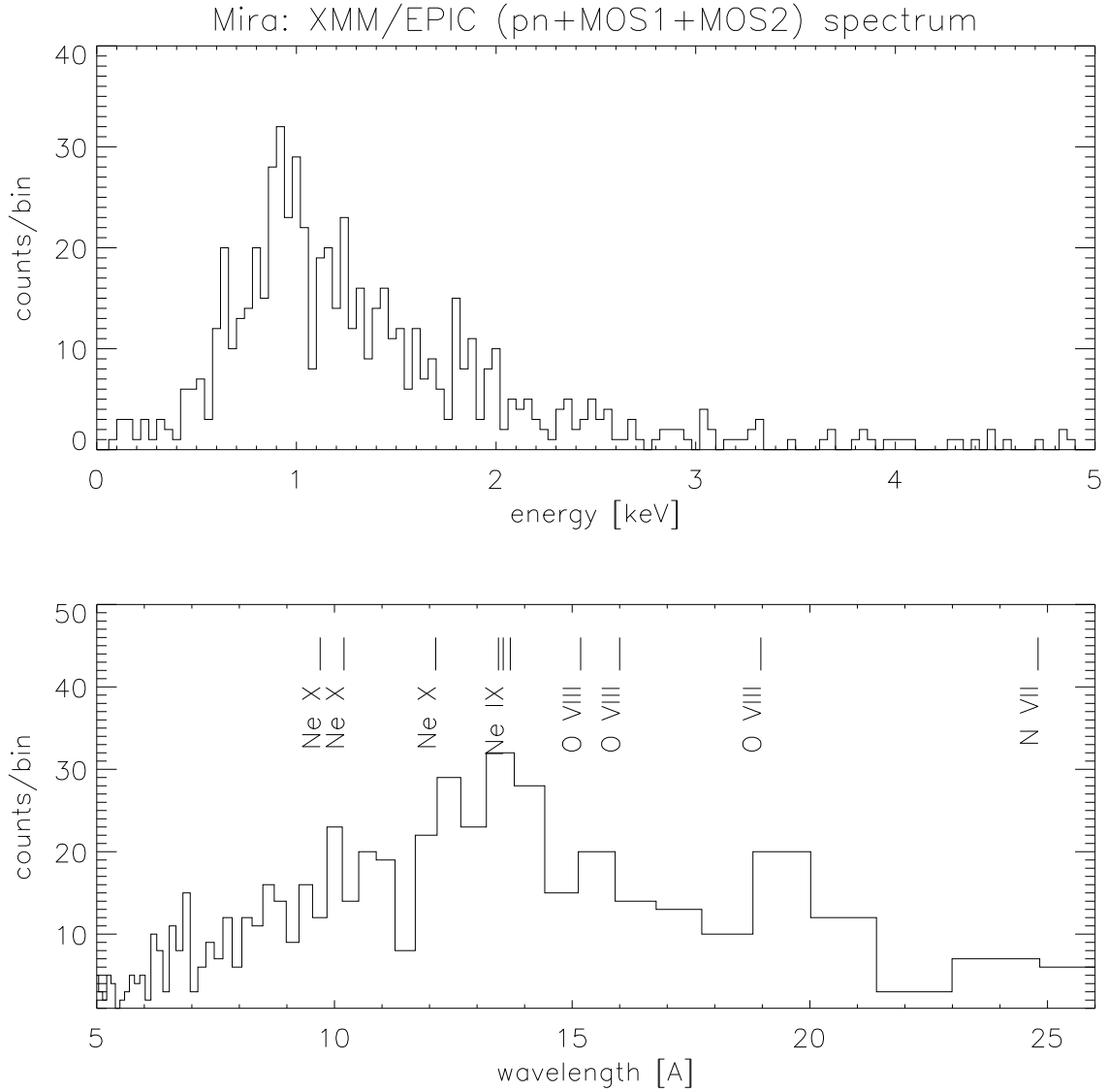
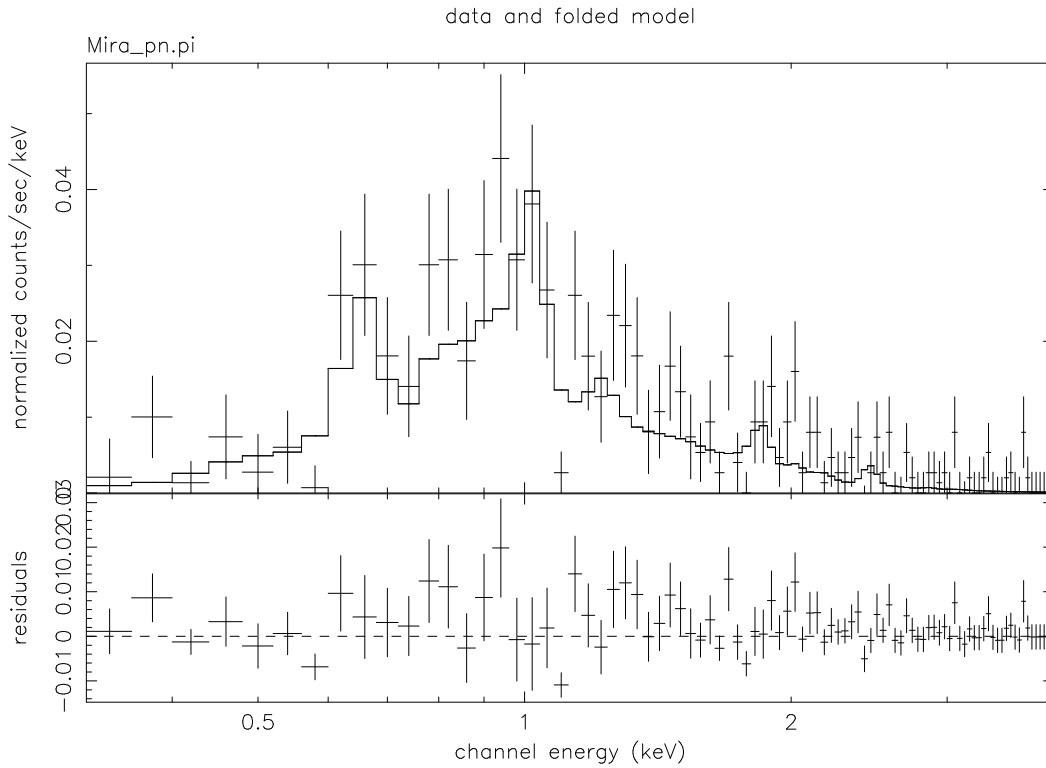


Fig. 1.— Combined EPIC (MOS1, MOS 2, and pn) counts spectrum of the Mira system, plotted in 40 eV bins, as a function of energy (top) and wavelength (bottom). Positions of prominent lines of highly ionized N, O, and Ne are indicated in the bottom panel.



20-Apr-2004 14:18

Fig. 2.— EPIC pn spectrum of the Mira system (crosses), with best-fit VMEKAL model overlaid (histogram). This best-fit model is obtained for  $N_H = 4.5 \times 10^{21} \text{ cm}^{-2}$  and  $kT_X = 0.83 \text{ keV}$ , with highly elevated O abundance (see text).

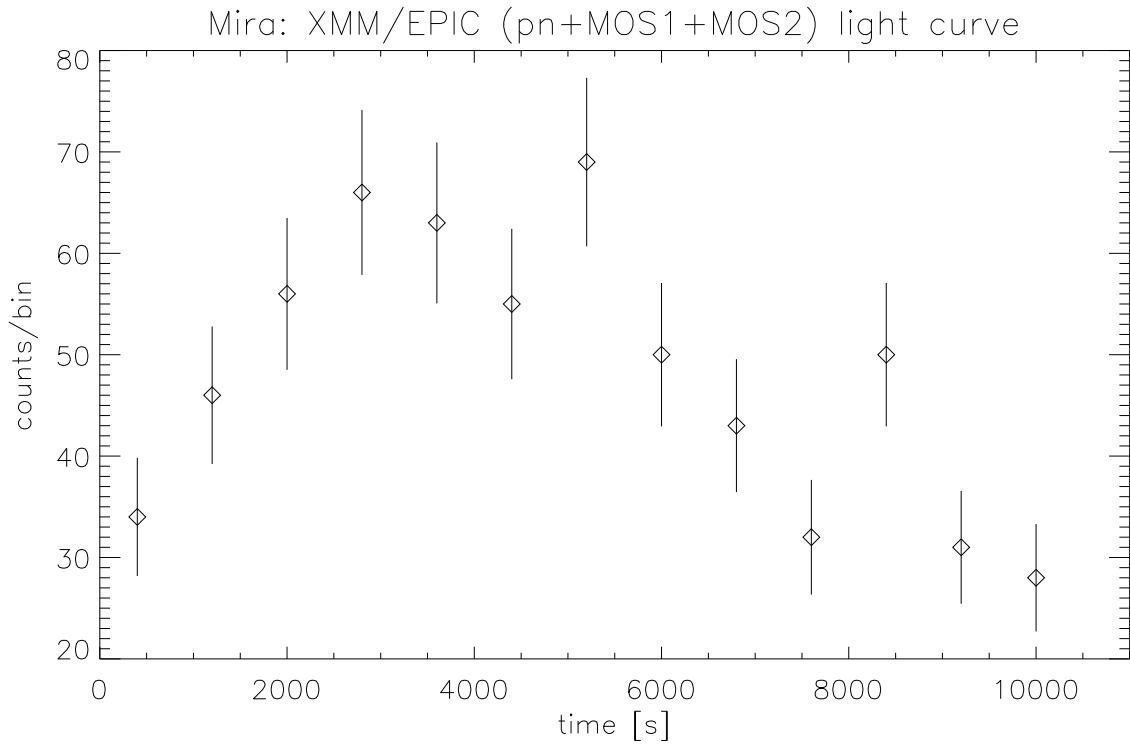


Fig. 3.— Combined EPIC (MOS1, MOS 2, and pn) light curve of the Mira system. Time bins are 800 s and the time interval is confined to the 10.4 ks period of active integration by all three instruments.